Proceedings of the 16th International Heat Transfer Conference, IHTC-16
August 10-15, 2018, Beijing, China

IHTC16-22301

TURBULENT FORCED CONVECTION IN POROUS MEDIA: A DIRECT NUMERICAL SIMULATION STUDY

Stefan Gasow[1], Andrey V. Kuznetsov[2], Michael Schlüter[1], Yan Jin[3*]

[1] Institute of Multiphase Flows, Hamburg University of Technology, Hamburg, Germany, D-21073
[2] Department of Mechanical and Aerospace Engineering, North Carolina State University, Raleigh, North Carolina 27695-7910, USA
[3] 2 Center of Applied Space Technology and Microgravity (ZARM), the University of Bremen, Bremen, 28359, Germany

ABSTRACT

Forced convection in porous media has many important applications, one of which is in thermal energy storage systems that use low cost materials, such as stones or brick, as heat storage materials. Turbulence is welcomed in such thermal energy storage systems since it efficiently enhances heat transfer. Forced convection in porous media can be described by the macroscopic momentum and energy equations. In order to close the macroscopic equations, we analyzed the microscopic flow and temperature fields in porous media by direct numerical simulation (DNS) methods. Two DNS methods were adopted in our study to compare and verify the results. They are a finite volume method (FVM) and a Lattice-Boltzmann method (LBM). The porous matrix is made of a large number of periodically arranged 3-dimensional spheres. Based on our DNS results, we proposed a macroscopic model for calculating forced convection in porous media.

KEY WORDS: Porous medium, Forced convection, Turbulence, Direct numerical simulation, Nusselt number

1. INTRODUCTION

A porous medium refers to a material consisting of a solid matrix with interconnected voids. Examples of porous media are sandstone, soil, coal, brick, and fiberglass. Fluid flows in porous media often occur at low velocities and are thus laminar. However, when the Reynolds number, defined based on the size of the matrix elements, d, and the mean flow velocity, u_m, is of the order of 100 or higher, the flow within the pores becomes turbulent.

Turbulence is welcomed in many industrial applications because it enhances heat and mass transfer. A thermal energy storage system can be used to demonstrate the significance of turbulent porous medium flow. Rocks/bricks are often used for storing thermal energy. Although they come at a low cost, these materials have low thermal conductivity, leading to a very slow charging and discharging process. To overcome this limitation, the porous element size and the mean velocity may be adjusted to make the flow fully turbulent. For a tube bank (which can be approximated as a porous medium), a relationship between the Nusselt number and the Reynolds number changes from $Nu \sim Re^{0.36}$ for $Re<300$ to $Nu \sim Re^{0.64}$ for a fully turbulent flow ($Re>300$) [1]. Heat transfer is thus efficiently enhanced by transition to turbulence.

For engineering applications, it is more practical to solve macroscopic equations to simulate turbulent flows and heat transfer in porous media since using microscopic simulations requires the specification of a detailed geometry of the porous matrix and also is computationally very expensive. In order to close the volume-averaged Reynolds stress and temperature fluctuation terms in the macroscopic equations, various turbulence models have been developed. The so-called eddy viscosity assumption is commonly adopted in most models

*Corresponding Author: yan.jin@zarm.uni-bremen.de

to calculate the Reynolds stress. Representative models are those developed by Lee & Howell [2], Prescott & Incropera [3], Antohe & Lage [4], and de Lemos & Pedras [5].

However, the eddy viscosity assumption was developed for clear fluid flows (with no solid obstacles) and thus its validity for porous medium flows needs to be proven. In our recent direct numerical simulation (DNS) studies, we found that the size of turbulent structures in a porous medium is generally limited by the pore size, which leads to the pore scale prevalence hypothesis (PSPH) [6-8]. This is in accordance with the hypothesis proposed by Nield [9, 10], which states that true macroscopic turbulence, at least in a dense porous medium, is impossible because of the limitation on the size of turbulent eddies imposed by the pore scale.

The purpose of the present study is to develop a model for turbulent forced convection in a porous medium. Forced convection in a generic porous matrix (GPM) composed of a large number of spheres will be studied with DNS methods. The DNS results will be used to further validate the PSPH, propose a macroscopic model for a turbulent flow in a porous medium, and determine its coefficients. The proposed macroscopic model will also account for local thermal non-equilibrium (LTNE) effects.

2. GOVERNING EQUATIONS AND NUMERICAL METHODS

2.1 Microscopic and macroscopic equations

Forced convection in a porous medium in a heat storage system is typically characterized by local thermal non-equilibrium. The microscopic governing equations are incompressible Navier-Stokes and energy conservation equations. In Cartesian coordinates these equations are

$$\frac{\partial u_i}{\partial x_i} = 0 \tag{1}$$

$$\frac{\partial u_i}{\partial t} + \frac{\partial (u_i u_j)}{\partial x_j} = -\frac{\partial p}{\partial x_i} + \nu \frac{\partial^2 u_i}{\partial x_j^2} + g_i \tag{2}$$

$$\frac{\partial T_f}{\partial t} + \frac{\partial (u_i T_f)}{\partial x_j} = \alpha_f \frac{\partial^2 T_f}{\partial x_j^2} \tag{3}$$

$$\frac{\partial T_s}{\partial t} = \alpha_s \frac{\partial^2 T_s}{\partial x_j^2} \tag{4}$$

where ν is the kinematic viscosity of the fluid; α_f and α_s are the thermal diffusion coefficients of the fluid and the solid matrix, respectively; T_f and T_s are the fluid and solid temperatures, respectively; and g_i is a constant applied pressure gradient which causes the fluid flow. The viscous heat dissipation is neglected in the thermal energy conservation equation (3).

By performing time and volume averaging of Eqs. (1) and (2) over a representative elementary volume (REV), of Eq. (3) over the fluid part of the REV, and of Eq. (4) over the solid part of the REV, we obtained the following macroscopic equations:

$$\frac{\partial (\phi \langle \bar{u}_i \rangle^i)}{\partial x_i} = 0 \tag{5}$$

$$\frac{\partial (\phi \langle \bar{u}_i \rangle^i)}{\partial t} + \frac{\partial (\phi \langle \bar{u}_i \rangle^i \langle \bar{u}_j \rangle^i)}{\partial x_j} + \frac{\partial (\phi \langle {}^i\bar{u}_i {}^i\bar{u}_j \rangle^i)}{\partial x_j} = -\frac{\partial (\phi \langle \bar{p} \rangle^i)}{\partial x_i} + \nu \frac{\partial^2 \phi \langle u_i \rangle^i}{\partial x_j^2} - \frac{\partial \left(\phi \langle \overline{u_i' u_j'} \rangle^i\right)}{\partial x_j} + \phi g_i + \bar{R}_i \tag{6}$$

$$\frac{\partial \langle \bar{T}_f \rangle^i}{\partial t} + \frac{\partial \left(\phi \langle \bar{u}_i \rangle^i \langle \bar{T}_f \rangle^i\right)}{\partial x_i} + \frac{\partial \left(\phi \langle {}^i\bar{u}_i {}^i\bar{T} \rangle^i\right)}{\partial x_i} = -\frac{\partial \left(\phi \langle \overline{u_i' T_f'} \rangle^i\right)}{\partial x_i} + a_{fm} \frac{\partial^2 \langle \bar{T}_f \rangle^i}{\partial x_i^2} + \frac{\dot{q}'''}{\rho c_p} \tag{7}$$

$$\frac{\partial \langle \bar{T}_s \rangle^s}{\partial t} = a_{sm} \frac{\partial^2 \langle \bar{T}_s \rangle^s}{\partial x_i^2} - \frac{\dot{q}'''}{\rho_s c_s} \tag{8}$$

Here ϕ is the porosity of the porous matrix. The operator $\bar{}$ denotes time averaging, the operator $\langle \cdot \rangle^i$ denotes volume averaging over the fluid region of a REV, and the operator $\langle \cdot \rangle^s$ denotes volume averaging over the

solid region. The operator ${}^{i}\varphi$, where φ is any dependent variable, is defined as ${}^{i}\varphi = \varphi - \langle\varphi\rangle^{i}$. Parameters a_{fm} and a_{sm} are the thermal diffusivities of the fluid and solid phases of the porous medium, respectively, and $\dot{q}'''$ is the volumetric heat transfer rate from the solid matrix to the fluid. In order to close Eqs. (5)-(8), we studied convection in porous media with DNS methods and investigated the turbulence length scales.

2.2 Direct numerical simulation methods

Two different methods which complement and verify each other were utilized in this study to understand the mechanism of turbulence in porous media. They are

- The finite volume method (FVM) which directly solves the Navier-Stokes equations.
- The Lattice-Boltzmann method (LBM) which determines the particle distribution; this method indirectly corresponds to solving the Navier-Stokes equations.

In our FVM, the solution of Eqs. (1)–(3) was advanced in time with the second-order implicit backward method. Eq. (4) was not solved in our study because an isothermal boundary condition was used at the surfaces of the solid matrix. A second-order central difference scheme was used for spatial discretization. The pressure at the new time level was determined by the Poisson equation. The velocity was corrected by the pressure-implicit scheme with splitting of operators (PISO) pressure–velocity coupling.

The basic equation for the LBM is a discretized version of the Boltzmann equation [11] with the collision operator being treated by the Bhatnagar-Gross-Krook (BGK) model [12], i.e.

$$f_i(\mathbf{x} + \boldsymbol{\xi_i}\Delta t, t + \Delta t) - f_i(\mathbf{x}, t) = -\frac{1}{\tau}\Big(f_i(\mathbf{x}, t) - f_i^{eq}(\mathbf{x}, t)\Big) \tag{9}$$

where $\boldsymbol{\xi_i}$ is a discrete particle velocity, $f_i(\mathbf{x}, t)$ is the probability to find a particle with a velocity $\boldsymbol{\xi_i}$ at a position $\mathbf{x}$ at a time t, $f_i^{eq}(\mathbf{x}, t)$ is the equilibrium form of $f_i(\mathbf{x}, t)$, and τ is the relaxation time, which is related to the viscosity of the fluid. Different macroscopic velocities now correspond to different probability distributions of the particle velocities. A standard grid for modeling the three-dimensional motions of that kind, shown in Fig. 1, is called the D3Q19-grid (D3: three-dimensional, Q19: 19 discrete velocities). More details can be found in Chen & Doolen [13].

2.3 Techniques for detecting turbulence length scales

Turbulence is characterized by the fluctuating flow field quantities that are strongly affected by eddy structures of various sizes, often called coherent structures. These coherent structures are the building blocks of turbulence. These structures need to be identified when turbulence is analyzed in detail.

Here we used the two-point correlations to determine the length scale of the turbulent structures. A two-point correlation between the quantities $u_i'(\boldsymbol{x})$ and $u_j'(\boldsymbol{x} + \boldsymbol{r})$ at a certain time t is defined as:

$$R_{ij}(\boldsymbol{r}, \boldsymbol{x}) = \overline{u_i'(\boldsymbol{x}, t)\, u_j'(\boldsymbol{x} + \boldsymbol{r}, t)} \tag{10}$$

where $\bar{}$ denotes time (Reynolds) averaging. The length scale of the turbulent structures can be determined by the non-zero region of R_{ij}. However, non-zero correlations are not solely from turbulent fluctuations but also can be caused by simultaneous unsteady motions around each of the porous elements. They are called non-turbulent correlations and they have to be distinguished from the true turbulent correlations due to the turbulent coherent structures. This can be done provided the non-turbulent correlations are the same for all values r_3, i.e. the $u_i'(\boldsymbol{x_0}, t)$ correlation and $u_j'(\boldsymbol{x_0} + \boldsymbol{r} + r_3\boldsymbol{e_3}, t)$ correlation have the same non-turbulent correlation pattern. Adding $r_3\boldsymbol{e_3}$ to the correlation distance $\boldsymbol{r}$ means that now the correlation points are located in two parallel planes which are a distance r_3 apart, see Fig. 2. We call this special correlation a two-point lateral correlation; it is defined as:

$$\tilde{R}_{ij}\,(r_3, \boldsymbol{r}, \boldsymbol{x}) = \overline{u_i'(\boldsymbol{x}, t)\; u_j'\,(\boldsymbol{x} + \boldsymbol{r} + \; r_3 \boldsymbol{e_3}, t)} \tag{11}$$

When the quantity $\tilde{R}_{ii}$ is subtracted from R_{ii} defined by Eq. (10), the difference

$$\hat{R}_{ij} = R_{ij} - \; \tilde{R}_{ij} \tag{12}$$

corresponds to the true turbulent correlations provided r_3 is so large that there are no correlations due to the large-scale turbulent structures in $\tilde{R}_{ij}$.

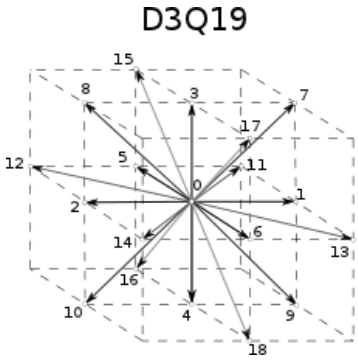

Fig. 1 Grid structure and velocities with the D3Q19 discretization.

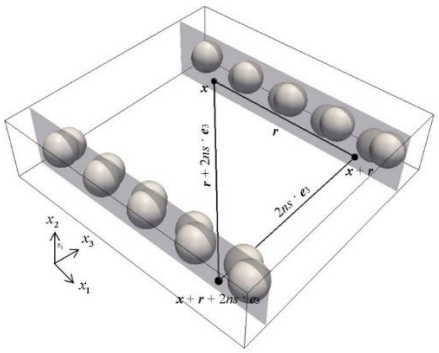

Fig. 2 Correlation points in two parallel planes

3. GENERIC POROUS MATRIX

The generic porous matrix (GPM) is composed of aligned distributed spheres with the diameter *d* and distance *s* apart from each other. The GPM used in this study and the representative elementary volume (REV) are shown in Fig. 3. Periodic boundary conditions are used in all three directions. Fluid flow and heat transfer are produced by a constant applied pressure gradient g_i and a constant temperature difference ΔT in the x_1 direction, i.e. $T(0, x_2, x_3) + \Delta T = T(L_1, x_2, x_3)$, where L_1 is the length of the domain. The bulk temperature of each REV is calculated according to our DNS results. Two values of the pore size *s*, 1.0 and 1.1, were adopted. Their corresponding porosity values are 0.48 and 0.61.

4. RESULTS AND DISCUSSIONS

4.1 Accuracy of DNS methods

Our DNS methods have already been verified by solving problems involving turbulent flow in porous media, see our studies in [6-8]. Here we focused on the mesh independence of our DNS results. Direct numerical simulation solutions need numerical grids that are fine enough to resolve the smallest scales involved. Quite generally these smallest scales are of the order of the Kolmogorov scale $\eta = \nu^{3/4}/\varepsilon^{1/4}$. A perfect DNS solution would comply with the condition $\Delta x_i/\eta \leq 1$, where Δx_i are the mesh sizes in the three dimensions of the solution domain. Since η is not uniformly distributed, we compare our mesh sizes with the mean Kolmogorov scale η_m for the flow domain. A typical FVM case has 270,000 cells in each REV and 9.72 million cells in total. The mesh is concentrated near the wall. $\Delta x_w/\eta_m$ is smaller than 0.1, where Δx_w is the distance from the first cell to the wall. The largest $\Delta x_i/\eta_m$ is smaller than 10. Uniformly distributed meshes were used for our LBM cases. The case with the highest Reynolds number has 680,000 cells in each REV and 174 million cells in total. The $\Delta x_i/\eta_m$ values for all the LBM cases are smaller than 2. However, we were still unable to achieve $\Delta x_i/\eta \leq 1$ everywhere in the flow domain, especially very close to the solid walls where the local dissipation rate ε is very large. Our simulations should therefore be considered as "low resolution DNS".

However, we found that our mesh resolution is sufficient to calculate parameters such as the friction coefficient and the Nusselt number correctly, which are of the primary interest for the present study. The friction coefficient and the Nusselt number only change slightly when the mesh resolution is increased.

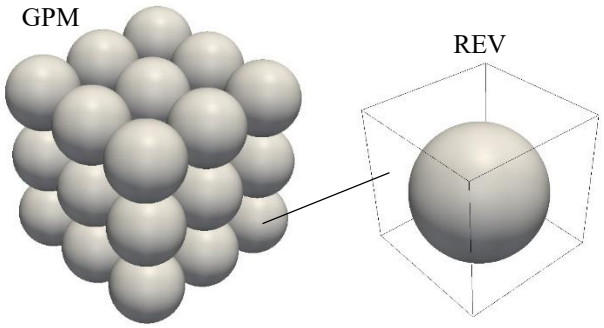

Fig. 3 Generic porous matrix (GPM) used in our study; 96 ($8 \times 4 \times 4$) REVs were used for the LBM simulations and 36 ($4 \times 3 \times 3$) REVs were used for the FVM simulations.

4.2 Turbulent length scales and the PSPH

Fig. 4 shows the instantaneous velocity field and the vortical structures identified by the iso-surfaces of Q. The quantity Q is the second invariant of the instantaneous velocity gradient tensor, which is defined as $-\frac{1}{2}\frac{\partial u_i}{\partial x_j}\frac{\partial u_j}{\partial x_i}$. Fig. 5 shows the instantaneous temperature field and iso-surfaces of the thermal dissipation rate. The thermal dissipation rate is defined as $k_f \frac{\partial T_f}{\partial x_i}\frac{\partial T_f}{\partial x_i}$. The thermal dissipation rate corresponds to the entropy generation rate in the temperature field when the temperature variation is small. It also corresponds to the entransy dissipation rate, which was proposed recently by Guo [14]. Jin and Herwig [15] argued that the thermal dissipation rate will be associated with certain sizes of vortical structures since it indicates the conversion rate of mechanical energy into internal energy. Figs. 4b and 5b show that turbulent structures are of the pore size or smaller with some of them reaching into neighboring pores but not further.

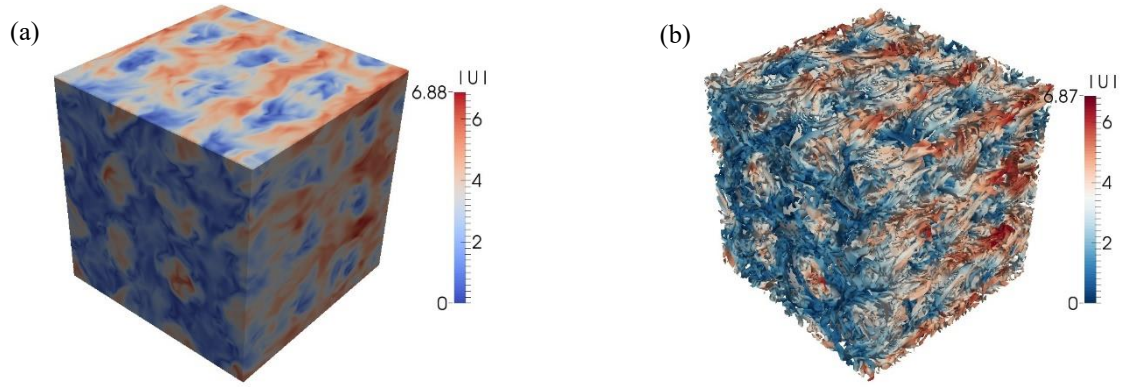

Fig. 4 Instantaneous flow fields, Re=342, LBM results. (a) Velocity magnitude; (b)Vortical structures identified by iso-surfaces of Q.

In Fig. 6 the two-point correlations R_{11}, $\tilde{R}_{11}$, and $\hat{R}_{11}$, computed according to Eqs. (10)-(12), are shown. In both cases ($\phi = 0.48$ and 0.61) non-zero turbulent correlations can be found only within a distance s away from the correlation point. R_{11} is almost identical to $\tilde{R}_{11}$ when the flow is laminar. Our DNS results confirmed the pore scale prevalence hypothesis (PSPH), i.e., that the size of turbulent eddies is restricted by the pore size.

4.3 A preliminary macroscopic model for turbulent convection in porous media

According to the PSPH, the effects of turbulence are confined within each REV, thus Eqs. (5)-(8) can be simplified to

$$\frac{\partial(u_{Di})}{\partial x_i} = 0 \tag{13}$$

$$\frac{\partial(u_{Di})}{\partial t} + \frac{\partial(u_{Di}u_{Di}/\phi)}{\partial x_j} = -\frac{\partial p_D}{\partial x_i} + \phi g_i + \bar{R}_i \tag{14}$$

$$\frac{\partial T_{fD}}{\partial t} + \frac{\partial(u_{Di}T_{fD})}{\partial x_i} = \tilde{a}_{fm}\frac{\partial^2 T_{fD}}{\partial x_i^2} + \frac{\dot{q}'''}{\rho c_p} \tag{15}$$

$$\frac{\partial T_{sD}}{\partial t} = a_{sm}\frac{\partial^2 T_{sD}}{\partial x_i^2} - \frac{\dot{q}'''}{\rho c_p} \tag{16}$$

where $u_{Di} = \phi\langle\bar{u}_i\rangle^i$ is the superficial velocity, $p_D = \phi\langle\bar{p}\rangle^i$ is the mean pressure, $T_{fD} = \langle\bar{T}_f\rangle^i$ is the mean temperature in the fluid region, and $T_{sD} = \langle\bar{T}_s\rangle^s$ is the mean temperature in the solid region. The time averaged drag $\bar{R}_i$ can be modeled by the Brinkman-Forchheimer extension of the Darcy law, i.e.

$$\bar{R}_i = -\phi(\bar{R}_{Di} + \bar{R}_{Fi} + \bar{R}_{Bi}) = -\phi\left(\frac{\nu}{K}\cdot u_{Di} + \frac{C_F}{\sqrt{K}}|\mathbf{u}_D|\cdot u_{Di} - \frac{\partial}{\partial x_j}\left(\tilde{\nu}\frac{\partial u_{Di}}{\partial x_j}\right)\right) \tag{17}$$

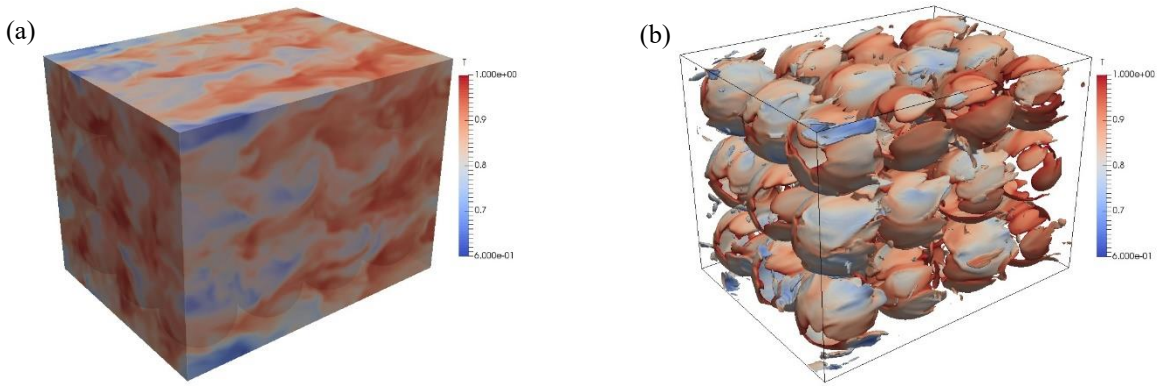

Fig. 5 Instantaneous heat transfer field, Re=610, FVM results. (a) Temperature T_f; (b) Iso-surfaces of the thermal dissipation rate $k_f\frac{\partial T_f}{\partial x_i}\frac{\partial T_f}{\partial x_i}$.

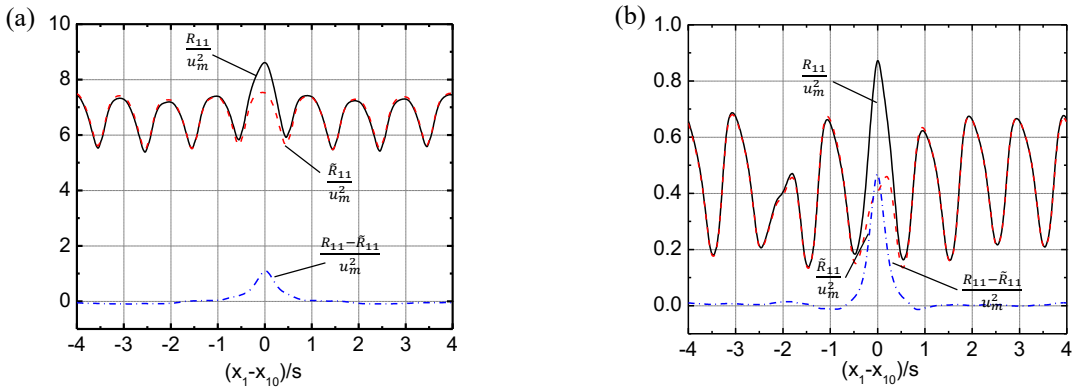

Fig. 6 Two-point correlations. (a) $\phi = 0.48$, Re=342; (b) $\phi = 0.61$, Re=566. $\mathrm{Re} = u_m K^{1/2}/\nu$ is the Reynolds number, where u_m is the mean flow velocity.

The permeability K is calculated according to the Kozeny's equation [10]:

$$K = \frac{d^2\phi^3}{\beta(1-\phi)^2} \tag{18}$$

where the coefficient β is 140. The model coefficient C_F was determined according to our DNS results. Fig. 7 shows the relationship between the friction coefficient $f_k = K^{1/2}(dp/dx)/\rho u_m^2$ and the Reynolds number $\mathrm{Re}_K = u_m K^{1/2}/\nu$. The discrepancies between the FVM and LBM results are mainly due to the uncertainties of the numerical solutions of a nonlinear system. Also, the LBM equations are only an approximation of the

incompressible Navier-Stokes equations. Different initial fields may lead to uncertainties in the transition region. Despite of these discrepancies, f_k can be reasonably well approximated by

$$f_K = \frac{1}{\mathrm{Re}_K} + 0.105 \tag{19}$$

which indicates that the coefficient C_F is 0.105. This qualitatively agrees with [10], which states that C_F ranges from 0.1 to 0.55. The parameter $\tilde{\nu}$ is an effective viscosity involved in the Brinkman's term. Vafai and Tien [16] suggested that $\tilde{\nu}$ can be approximated as ν/ϕ. However, in our recent study, we found that $\tilde{\nu}$ is proportional to $s^2\left|\frac{\partial u_{Di}}{\partial x_j}\right|$ at large Reynolds numbers, where s is the pore size. According to [17], the effective thermal diffusivity $\tilde{a}_{fm}$ can be calculated as

$$\tilde{a}_{fm} = a_{fm} + \gamma K^{1/2}|u| \tag{20}$$

where the coefficient γ has a value of 0.025. The parameters a_{fm} and a_{sm} can be approximated by ϕa_f and $(1-\phi)a_s$, respectively, and $\dot{q}'''$ is calculated as

$$\dot{q}''' = \alpha A'''\left(T_{fD} - T_{sD}\right) \tag{21}$$

where A''' is the solid surface area per unit volume, and α is the heat transfer coefficient. The parameter α can be calculated from the local Nusselt number, $1/\alpha = d/\left(\mathrm{Nu}k_f\right) + d/(\beta k_s)$. The constant β is 10 [9]. Nu can be correlated with Re_K and the Prandtl number Pr as follows:

$$\mathrm{Nu} = A\mathrm{Re}_K^m \mathrm{Pr}^n \tag{22}$$

Fig. 8 shows the relationship between the Nusselt number Nu and Re_K at various Prandtl numbers. The DNS results indicate that the Nusselt number can be well fitted by Eq. (22) with $A = 3.6$, $m = 0.57$, and $n = 0.37$, which is close to the parameter values suggested in [10].

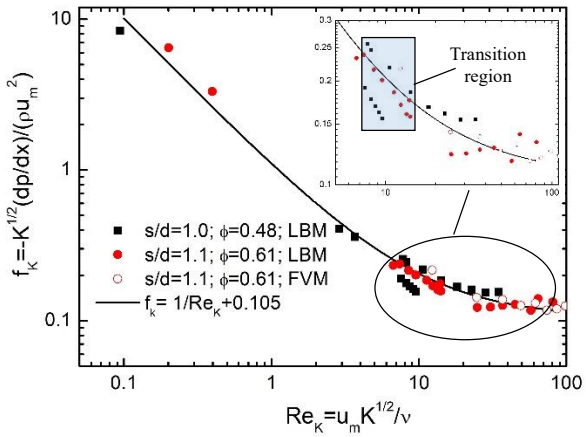

Fig. 7 Friction coefficient f_K at various porosities and Reynolds numbers.

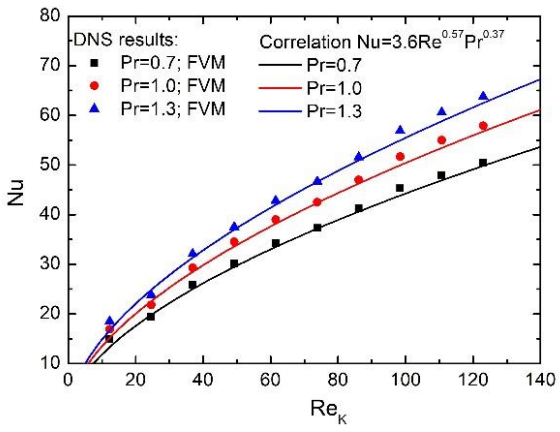

Fig. 8 Nusselt number Nu at various Prandtl and Reynolds numbers, $\phi = 0.61$.

5. CONCLUSIONS

We performed a direct numerical simulation study of turbulent forced convection in a porous medium composed of aligned spheres. We also validated the pore scale prevalence hypothesis (PSPH). Based on the PSPH we proposed a macroscopic model for forced convection in porous media. The model coefficients were determined from our DNS results. The effects of local thermal non-equilibrium are taken into account in the macroscopic model.

ACKNOWLEDGMENT

The authors gratefully acknowledge the support of this study by the DFG (Deutsche Forschungsgemeinschaft) and the computing center of Hamburg University of Technology (RZ-TUHH). AVK acknowledges with gratitude the support of the National Science Foundation (award CBET-1642262) and the Alexander von Humboldt Foundation through the Humboldt Research Award.

NOMENCLATURE

a_e	effective thermal diffusivity (m^2s^{-1})	C_F	constant in the Forchheimer's term (-)
a_m	thermal diffusivity of a porous medium (m^2s^{-1})	K	permeability (m^2)
		Nu	Nusselt number (-)
R_i	time averaged drag (ms^{-2})		(ms^{-1})
R_{ij}	two point correlation (m^2s^{-2})	ϕ	porosity (-)
Re	Reynolds number (-)	α	heat transfer coefficient ($Wm^{-2}K^{-1}$)
Pr	Prandtl number (-)	$\tilde{v}$	effective diffusivity (m^2s^{-1})
u_{Di}	superficial velocity	γ	temperature dispersion coefficient (-)

Subscripts

f	fluid	s	solid

REFERENCES

[1] Engineering Sciences Data Unit, "Low-fin Staggered Tube Banks: Heat transfer and Pressure Drop for Turbulent Single Phase Cross Flow," *Engineering Sciences Data Unit*, ESDU Data Item No. 84016, (1984).

[2] Lee, K. B. and Howell, J. R., "Theoretical and experimental heat and mass transfer in highly porous media," *Int. J. Heat Mass Transfer*, 34(8), pp. 2123-2132, (1991).

[3] Prescott, P.J. and Incropera, F. P., "The effect of turbulence on solidification of a binary metal alloy with electromagnetic stirring," *ASME J. Heat Transfer*, 117(3), pp. 716-724, (1995).

[4] Antohe, B. V. and Lage, J. L., "A general two-equation macroscopic turbulence model for incompressible flow in porous media," *Int. J. Heat Mass Transfer*, 40(13), pp. 3013–3024, (1997).

[5] de Lemos, M. J. S. and Pedras, M. H. J., "Recent mathematical models for turbulent flow in saturated rigid porous media," *ASME J. Fluids Engineering*, 123(4), pp. 935-940, (2001).

[6] Jin, Y., Uth, M.-F., Kuznetsov, A. V. and Herwig, H., "Numerical investigation of the possibility of macroscopic turbulence in porous media: a DNS study," *J. Fluid Mechanics*, 766, pp. 76-10, (2015).

[7] Uth, M.-F., Jin, Y., Kuznetosov, A.V. and Herwig, H., "A DNS study on the possibility of macroscopic turbulence in porous media: effects of different solid matrix geometries, solid boundaries, and two porosity scales," *Phys. Fluids*, 28(6), pp. 065101, (2016).

[8] Jin, Y. and Kuznetosov, A.V., "Turbulence modeling for flows in wall bounded porous media: An analysis based on direct numerical simulations," *Phys. Fluids*, 29(4), pp. 045102, (2017).

[9] Nield, D. A., "Alternative models of turbulence in a porous medium, and related matters," *ASME J. Fluids Engineering*, 123(4), pp. 928-931, (2001).

[10] Nield, D. A. and Bejan, A., *Convection in Porous Media,* New York: Springer-Verlag, (2017).

[11] Aidun, C. K. and Clausen, J. R., "Lattice-Boltzmann Method for Complex Flows," *Annu. Rev. Fluid Mech*, 42, pp. 439-472, (2010).

[12] Bhatnagar, P. L., Gross, E. P. and Krook, M., "A Model for Collision Processes in Gases. I. Small Amplitude Processes in Charged and Neutral One-Component Systems," *Physical Review*, 94(3), pp. 511-525, (1954).

[13] Chen, S. and Doolen, G. D., "Lattice Boltzmann Method for Fluid Flows," *Annu. Rev. Fluid Mech*, 30(1), pp. 329-364, (1998).

[14] Guo, Z. Y., Zhu, H. Y., and Liang, X. G., "Entransy—A physical quantity describing heat transfer ability," *Int. J. Heat Mass Transfer*, 50(13–14), pp. 2545-2556, (2007).

[15] Jin, Y. and Herwig, H., "From single obstacles to wall roughness: Some fundamental investigations based on DNS results for turbulent channel flow," *J. Applied Mathematics and Physics*, 64(4), pp. 1337-1352, (2013).

[16] Vafai, K. and Tien, C. L., "Boundary and inertial effects on convective mass transfer in porous media," *Int. J. Heat Mass Transfer*, 25(8), pp. 1183–1190, (1982).

[17] Hunt, M. L. and Tien, C. L., "Effects of thermal dispersion on forced convection in fibrous media," *Int. J. Heat Mass Transfer*, 31(2), pp. 301–309, (1988).